PROCEEDINGS OF SPIE

Advances in X-Ray/EUV Optics and Components III

Ali M. Khounsary
Christian Morawe
Shunji Goto
Editors

11–13 August 2008
San Diego, California, USA

Sponsored and Published by
SPIE

Volume 7077

Proceedings of SPIE, 0277-786X, v. 7077

Bragg diffraction of a focused x-ray beam as a new depth sensitive diagnostic tool

A. Kazimirov*[a], V. G. Kohn[b], Z.-H. Cai[c]
[a]Cornell High Energy Synchrotron Source (CHESS), Cornell University, Ithaca, New-York, 14853;
[b]Russian Research Center "Kurchatov Institute", 123182 Moscow, Russia;
[c]Advanced Photon Source, 9700 S. Cass Avenue, Illinois, 60409

ABSTRACT

Results of the first experiment in which Bragg diffraction of a focused x-ray beam was utilized to obtain depth sensitive structural information are presented. Silicon-on-insulator (SOI) layers of 4.5 to 25 μm thick were studied. The beam was focused by a circular zone plate. A beam stop and an order sorting aperture were used to reduce the contribution of the background radiation into diffracted intensity. Diffraction patterns were recorded by a CCD detector placed in the focus of the zone plate. Spatial distributions of the recorded intensity in the scattering plane revealed variations of the lattice constant within the layers. Incoherent scattering was observed out of the scattering plane thus providing a new method to study diffuse scattering. Computer simulations of the intensity patterns produced by the interface between two layers with the lattice constant mismatch are presented.

Keywords: X-rays, Bragg diffraction, focusing, crystal layer, zone plate, depth sensitivity

INTRODUCTION

In the early 1970s, the theoretical analysis of the Bragg diffraction of a very narrow X-ray beam by crystals [1,2] revealed a very interesting phenomenon: the beam is reflected not only from the front (entrance) surface layer of a crystal but also from the bottom surface. The crystal bulk in between does not reflect the beam. This property was explained recently [3,4] in terms of a plane wave expansion of a narrow beam. The plane waves corresponding to the angular region of the total reflection are Bragg reflected within the extinction length beneath the entrance surface and exit the crystal. Other plane waves are reflected kinematically and their depth of reflection are inversely proportional to the angular deviation from the Bragg condition. These waves are still present in the bulk of the crystal but the reflection is absent due to destructive interference between the waves scattering from various depths. The bottom surface partially breaks this destructive interference and the reflection takes place again.

This effect has not been observed so far due to the obvious experimental difficulties: both, a narrow slit and a detector have to be placed very close to the front surface. Recently [3,4], a new approach was proposed. It is based on using focusing optics such as refractive lenses [5] or Fresnel zone plates [6] to produce a narrow beam, thus eliminating the need for a narrow slit. Moreover, since for a perfect crystal a symmetric reflection is equivalent to a reflection from a mirror, the detector can be placed at the focus and the crystal anywhere between the lens and the detector.

Theoretical simulations fully confirmed this idea. It was shown [4] that not only the bottom surface of a crystal can break up the destructive interference but any lateral defect or interface will have a similar effect. For example, a boundary between two layers with slightly different lattice spacing can be visualized as well. Therefore, this technique can be used as a new depth selective diagnostic tool for studying lateral defects inside crystals. Since the modern focusing optics can produce extremely small beams this technique allows one also to localize defects in very thin surface layers.

---

*ayk7@cornell.edu; phone (607)255-2538; fax (607)255-9001;

Advances in X-Ray/EUV Optics and Components III,
edited by Ali M. Khounsary, Christian Morawe, Shunji Goto,
Proc. of SPIE Vol. 7077, 70770L,(2008) · 0277-786X/08/$18 · doi: 10.1117/12.793750

This article presents the first experimental results obtained by this new technique. The article is organized as follows. Section 2 describes the experimental setup. The experimental results are discussed in Section 3. Computer simulations are presented in Section 4 followed by conclusions and perspectives on future.

EXPERIMENTAL SETUP

The experiment was performed at the diffraction microscopy beamline 2-ID-D at the Advanced Photon Source[7]. The experimental setup is shown in Fig. 1. The X-ray wave of the energy of 9.5 keV was selected from the undulator beam by the upstream double-crystal Si(111) monochromator (not shown). A gold Fresnel zone plate ZP with an outmost zone width of 100 nm and a focal length of F = 12.18 cm was located at the distance of z_0 = 74 m from the source. The slit S limited the beam to the size of the zone plate aperture of 160 μm. To reduce the background radiation incident on the sample such as the collimated beam transmitted through the ZP and the higher focusing orders, a 35 μm diameter beam stop BS and a 25 μm diameter order sorting aperture OSA were used. They are the important part of the setup as the crystal may reflect the unwanted background radiation strongly while the focused beam is reflected weakly.

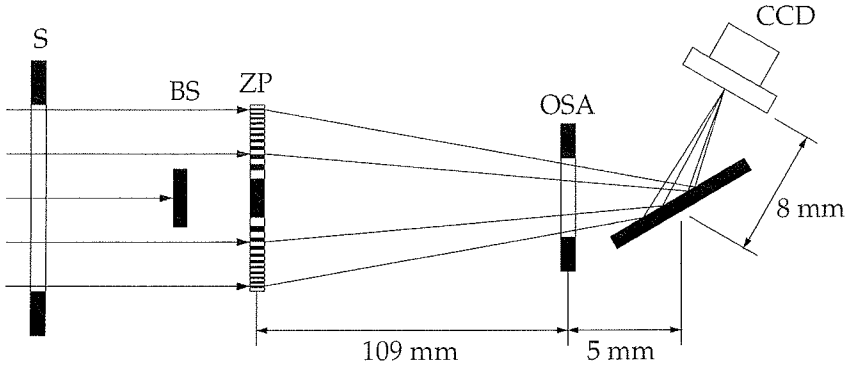

Fig. 1. The experiment setup. S is the slit, BS is the beam stop, ZP is the circular zone plate, OSA is the order sorting aperture, CCD is a high-resolution 2D detector. The sample was mounted on the sample stage of a six circle diffractometer, the CCD detector was mounted on the detector arm.

Beam size measurements were performed by using a knife edge (cleaved Si wafer with 200 Å Cr film) scan by recording the Cr-K fluorescence. The width of the Gauss fit was 0.43 μm. A typical size of the focused beam obtained with this zone plate at this energy is about 0.2 μm. The broadening might be due to the fact that the knife edge was installed on a detector arm and not on the sample stage, as usually, thus creating a vibration loop.

A high-resolution CCD camera had 1317 pixels horizontally and 1035 pixels vertically. A YAG doped film of 1.2 μm thick was used as a scintillator. With the objective used in this experiment the interpixel distance was 0.134 μm. The FWHM of the point spread function was measured as 1.5 μm by imaging the focused beam. The CCD camera was mounted on the detector arm of the six-circle diffractometer at the distance of $z_f = F/(1 - F/z_0)$ = 12.20 cm from the ZP. Samples were mounted on a sample stage with the axis of rotation at the distance of 8 mm from the detector. The diffraction images were recorded by the CCD detector at each angular point through the Bragg diffraction region by performing θ/2θ scans.

The samples were three thin silicon-on-insulator (SOI) layers[8] with the orientations and the thicknesses of (110) and 4.5 μm (#1); (111), 10 μm (#2); and (110), 25 μm (#3). The top layer was bonded to the Si substrate of the different orientation and thickness: (111), 480 μm (#1); (100), 500 μm (#2); (100), 525 μm (#3). A thin buried SiO_2 (box) layer was in between the SOI layer and the substrate with the thickness of 2 μm (#1), 1 μm (#2), and 0.5 μm (#3).

EXPERIMENTAL RESULTS

We explored the 220 symmetrical diffraction in the SOI layers of the samples #1 and #3 and the 111 symmetrical diffraction in the SOI layer of the sample #2. High-angular resolution diffraction performed at CHESS at the energy of

25.9 keV showed a noticeable broadening of the rocking curves with their shapes indicating a stepwise variation of the crystal lattice parameter inside the layers.

Diffraction curves measured from all three samples in the focused beam are shown in Fig. 2. The angular width of the ZP aperture was 270 arc sec which is much wider than the width of the rocking curves from the samples, typically about 25 arc sec as measured at CHESS at the energy of 10 keV, close to the energy of 9.5 keV used at the APS. Therefore, even not so perfect crystal as our SOI layers serves as an analyzer for the focused beam. The angular width of the curves is equal to the ZP aperture. The minimum observed on all three curves is due to the beam stop. The curve from the sample #1 (on the left) is the most symmetrical; the asymmetry of the middle curve from the sample #2 is most likely due to a slight misalignment of the beam stop relative to the ZP. We note that the minimum, even on the symmetrical diffraction curve on the left, is not very deep. This is because our circular ZP focuses X-rays in all directions whereas the crystal diffraction is not sensitive to the angular deviations normal to the scattering plane.

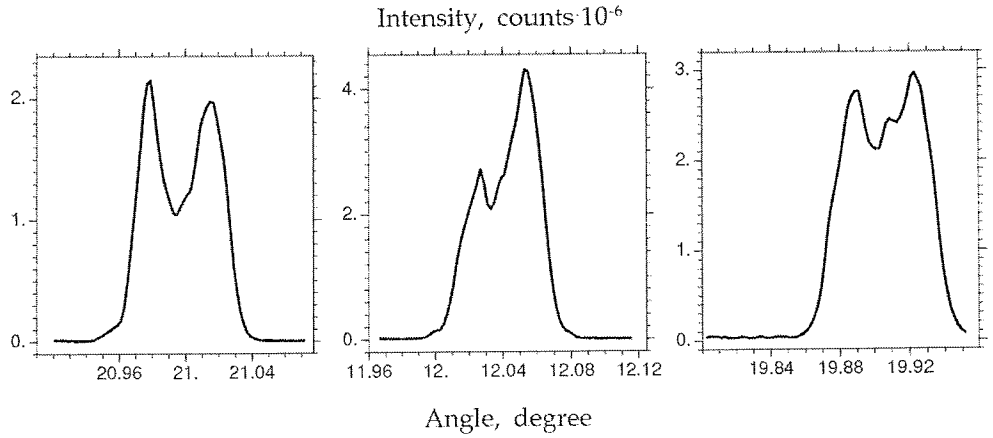

Fig. 2. Diffraction curves from all three samples measured in the beam focused by the circular zone plate: 220 diffraction from the samples #1 (left), 111 from #2 (middle), and 220 from #3 (right).

The spatial distribution of the focused-diffracted beam for each angular position of the sample was recorded by the CCD detector as a gray image of 16-bit per pixel. A typical image from the sample #2 is shown in Fig.3. The image was rotated by 90° to save the space so that the horizontal direction on this image is along the diffraction plane. The crystal does not affect focusing perpendicular to the diffraction plane and the image is sharp in that direction. In the diffraction plane the pattern is determined by the diffraction process. The strong main peak on the left corresponds to the reflection from the surface of the crystal. According to the theory[4] it is broadened due to the extinction effect and appears on the image as an elongated spot. A weak spot on the right is the reflection from the bottom surface. An additional intensity between these two spots we attribute to the imperfections in the layer.

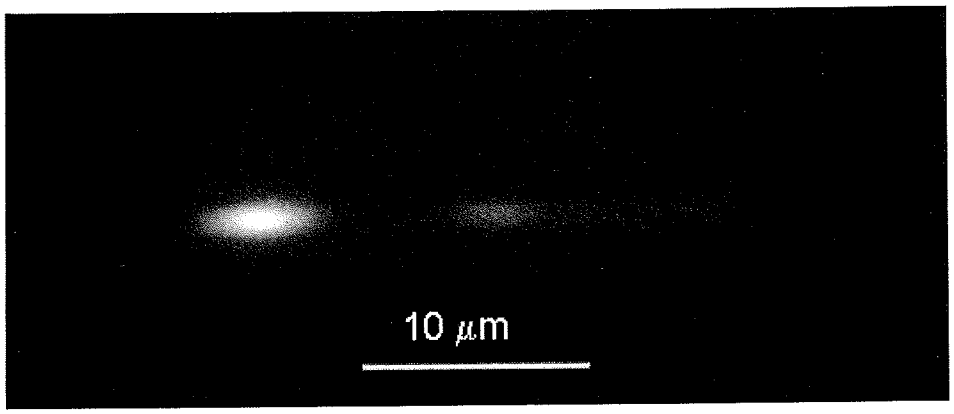

Fig. 3. CCD image of the spatial distribution of the focused beam diffracted from the sample #2 at one of the angular positions.

Intensity cross sections in the diffraction plane through the diffraction images for all angular positions were combined to produce a 3D map of the intensity distribution both in space and angle. Fig.4 shows such a map for the sample #3. The angular profile of the main peak which corresponds to the pixel region around 400 follows approximately the diffraction curve shown for this sample in Fig.2 on the right. The peak from the bottom surface is located around pixels 30 to 70. The middle peak which we attribute to the regions in the bulk with varying lattice constant is located in the pixel range of 140 to 300. The spatial position of this peak corresponds to the depth of the transition layer between the layers with different lattice constants.

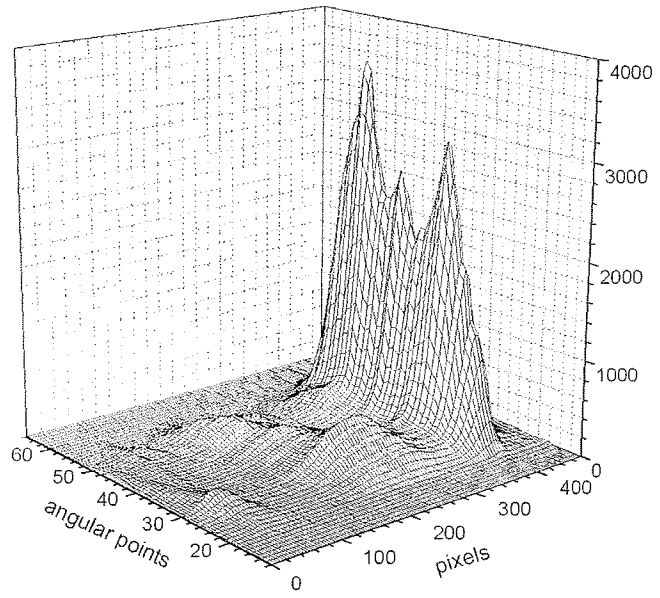

Fig. 4. A 3D map of the intensity distribution in space-angle for the sample #3 composed of the intensity cross sections from the individual CCD images recorded at the angular positions on the diffraction curve shown in Fig.2, right.

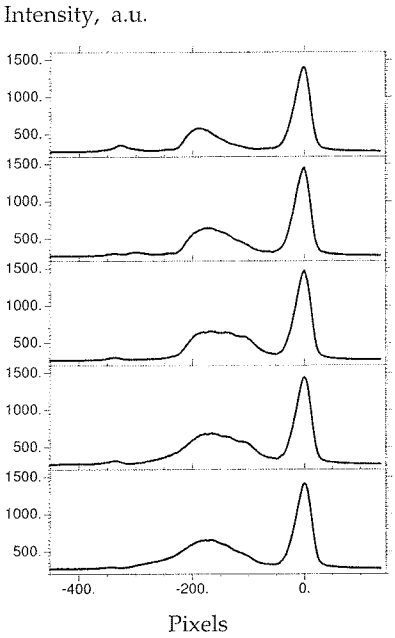

Fig. 5. Intensity cross sections measured at a fixed angular position while translating the sample in the direction perpendicular to the scattering plane with the step of 10 μm.

According to the theoretical simulations, the spatial position of the middle peak does not depend on the angular position on the diffraction curve. As we can see from the Fig.4, in our experiment this is not the case. While the reason for this effect is not entirely clear, here we can offer one possible explanation. The analysis of the images for all angles shows that the diffraction pattern is slightly shifting on the CCD screen as the sample is progressing through the Bragg diffraction region. This shift can be explained if we assume that the surface of the crystal was slightly off the axis of rotation. Then, each angular point would correspond to a slightly different position of the beam on the sample and, if the sample is not uniform laterally, this nonuniformity may show up on a 3D space-angle intensity distribution plot.

The lateral nonuniformity of the sample was evaluated by taking the CCD images at a fixed angular position while translating the sample laterally with a step of 10 μm in the direction perpendicular to the scattering plane. The intensity cross sections through the sequential diffraction images are shown in Fig. 5. Indeed, the shape of the middle peak is changing with the position on the sample from a more symmetrical peak on the bottom panel to the broadened plateau-like peak in the middle to a more sharp and asymmetrical peak on the top panel. One can see also that the peak from the bottom surface is also changing in intensity and shape. Thus, this peak is split to two weaker peaks on the second panel from the top indicating on a possible defect structure at the interface between the crystalline Si layer and the oxide box layer. These measurements may be viewed as the prototype of a future scanning depth-selective microscopy.

The main peak originates from the diffraction by a subsurface layer within the extinction length and it has the same shape for all positions. The theory [4] predicts a very sharp front edge for the peak which is determined by the size of the focused beam. In our experiment this is reflected in a slightly asymmetrical shape of the peak. The front edge is defined by the resolution of the setup which is determined mostly by the spatial resolution of the CCD detector. From the shape of the peak it can be estimated as about 2 micron.

So far we have considered only coherent scattering. It was shown theoretically [4] and confirmed in our experiment that the coherent scattering, i.e. the Bragg diffraction in our case, resulted in a spatial distribution of the scattering intensity in the scattering plane. In the direction normal to the scattering plane the focusing is not affected and the coherent intensity is concentrated within the same focal spot as without the crystal. The incoherent scattering, however, does not follow these principles. Fig.6 shows a spatial intensity pattern (in a log scale) recorded from the sample #3 at one of the angular positions. One can see the long intensity tails in the direction perpendicular to the scattering plane. This distribution cannot be explained by the point spread function of the CCD detector. We explain it as a diffuse scattering originating from the defects in the layer. It is well known that a lens (a zone plate) creates a Fourier image of the scattered radiation at the focal position. Then, each pixel in this image corresponds to a certain scattering vector defined by the pixel coordinates and the sample-to-focus distance. Therefore, this technique offers a new approach to measure diffuse scattering in a single shot for a whole range of scattering angles.

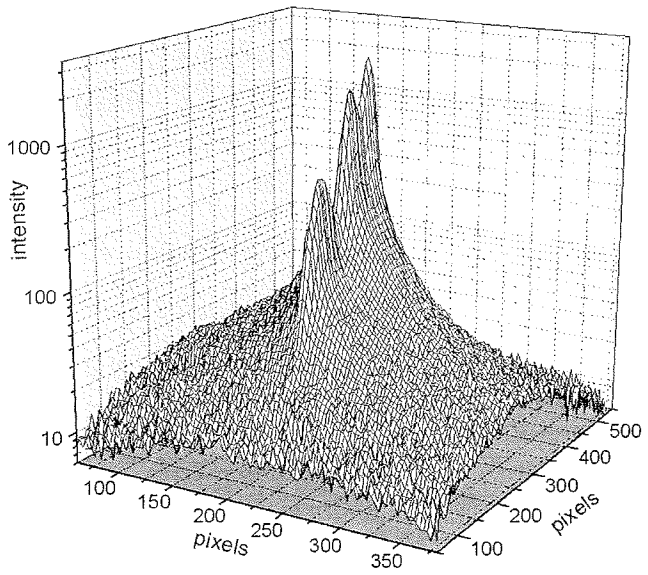

Fig. 6. Intensity pattern (in the logarithmic scale) recorded as a CCD image from the sample #2. Intensity tails in the direction perpendicular to the scattering plane originate from the diffuse scattering on defects.

COMPUTER SIMULATIONS

Let us assume that a two-dimensional wave function $\psi_0(x,y)$ of x-ray radiation is known in the plane of the OSA. We denote z_1 as the distance OSA-to-crystal and z_2 as the crystal-to-detector distance. The wave function $\psi_1(x,y)$ in the detector plane can be calculated in terms of a double Fourier transformation. In the first step we calculate the Fourier image $\Psi_0(q_x,q_y)$ of the known wave function. In the second step we obtain the unknown wave function as a Fourier integral

$$\psi_1(x,y) = C(x)\int\frac{dq_x dq_y}{(2\pi)^2}\Psi_0(q_x,q_y)P_r(q_x,z_t)P_r(q_y,z_t)R(q_x-q_0)\exp(iq_x[x-x_0]+iq_y y) \qquad (1)$$

Here $z_t = z_1 + z_2$, $R(q)$ is the crystal Bragg diffraction amplitude. Let φ be the angle of the crystal rotation, then

$$C(x) = \exp(2iK[\varphi x - \varphi^2 z_2]),\quad P_r(q,z) = \exp(-izq^2/2K),\quad K = 2\pi/\lambda,\quad q_0 = -K\varphi,\quad x_0 = 2\varphi z_2 \qquad (2)$$

The formula (1) is written in the paraxial approximation, $P_r(q,z)$ is the Fourier image of the Kirchhoff propagator. In real space, the propagation through air as well as the crystal diffraction have to be calculated as convolutions. The usage of the reciprocal space is convenient because all convolutions can be calculated as one integral.

The function $R(q)$ can be calculated for the case of a multilayer crystal as a result of successive application of the recurrent formula[4]. In this case we obtain $R(q)$ as $R_N(q)$ where

$$R_k(q) = \frac{A_1 - A_2 C \exp(i\alpha)}{1 - C\exp(i\alpha}, \quad C = \frac{A_1 - R_{k-1}(q)}{A_2 - R_{k-1}(q)}, \quad \alpha = \frac{a d_k}{\gamma_0}, \quad A_{1,2} = \frac{\sigma \pm a}{sf}, \tag{3}$$

$$\sigma = q\sin(2\theta_B) - i\mu_0, \quad a = (\sigma^2 - s^2 f)^{1/2}, \quad s = K\chi_h, \quad f = \chi_{-h}/\chi_h, \quad \mu_0 = K\chi_0''$$

Here d_k is the k-th layer thickness, χ_0, χ_h, and χ_{-h} are the Fourier components of the susceptibility of the crystal layer on the reciprocal lattice vectors 0, **h**, **-h**, the notation a'' means the imaginary part of the complex value a, and it is assumed that $a'' > 0$. The layers are numbered from the bottom to the top. Starting with $R_0(q) = 0$ and using the formulae (3) N times we obtain the final result.

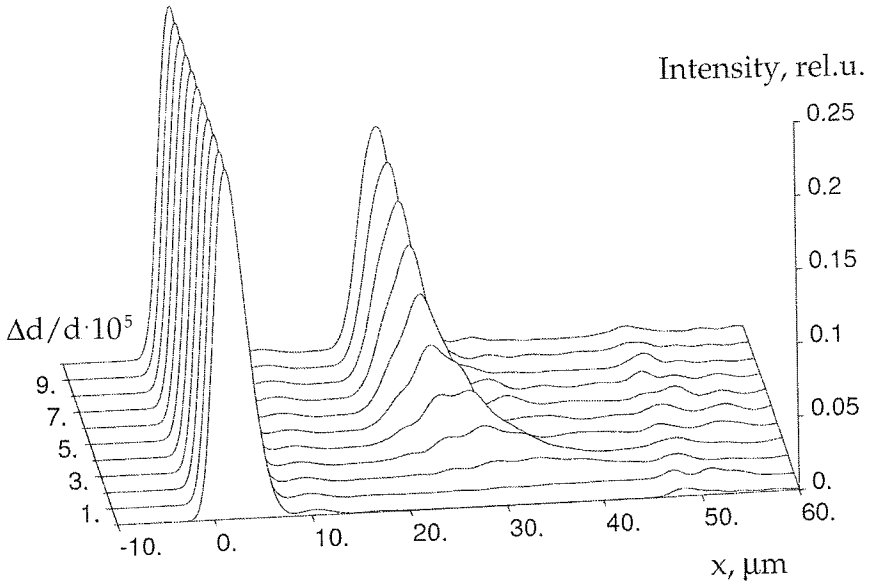

Fig. 7. Computer simulations of the interface between two layers with lattice mismatch: the 220 reflection, the energy is 9.5 keV, the total crystal thickness is 25 μm, and the position of the interface is at 10 μm below the surface. Simulations were performed for the linear zone plate.

We note that the wave function of the circular zone plate has a circular symmetry, so only the radial distribution has to be calculated. We can perform this calculation with a high accuracy. However, the integral (1) has no circular symmetry, therefore we need to calculate a two-dimensional Fourier integral with a high accuracy. Even when using a fast Fourier transformation (FFT) this is very difficult computational task because the number of points on the grid must be not less than 2^{26}. This is the reason why we performed our calculations with the linear zone plate. In this case, the function $\psi_0(x)$ does not depend on y coordinate, and the problem is reduced to the calculation of a one-dimensional integral.

We applied this approach to model an interface between two layers with different lattice constants. Calculations were performed for the 220 reflection, a energy of 9.5 keV, a crystal thickness of 25 μm, and the position of the interface at 10 μm below the surface. The spatial resolution of our experimental setup of 2 μm was also taken into account. Simulations were performed for the linear ZP. The result is shown in Fig.7. The lattice mismatch at the interface breaks up the destructive interference in the bulk of the layer which results in a peak with the intensity increasing with the lattice mismatch. The position of the peak is determined by the depth of the interface.

CONCLUSIONS

First experimental results reported in this article prove the depth sensitivity of the experimental setup, in which a sample is located between a focusing lens (zone plate) and its focus and a high resolution x-ray detector is located in the focus, predicted by theoretical simulations [4] based on linear refractive lenses. It was found that the use of circular focusing

optics in this setup offers a new approach to measure diffuse scattering in a single shot simultaneously for all scattering angles. Our results indicate that the SOI layers used in our experiment are not uniform but rather are composed of layers with varying lattice constant. Computer simulations confirmed the possibility of localizing the interface between two layers with a lattice constant mismatch. Future work will be directed towards expanding this technique to other focusing optics such as linear zone plates, linear and circular refractive lenses; improving the accuracy, stability and spatial resolution of the setup; performing computer simulations with both linear and circular zone plates and comparing them with experimental results from model samples.

ACKNOWLEDGEMENTS

This work is based upon research conducted at the Cornell High Energy Synchrotron Source (CHESS) which is supported by the National Science Foundation and the National Institutes of Health/National Institute of General Medical Sciences under NSF award DMR-0225180. The work of V.G.K. was supported by RFBR Grant Nos. 07-02-00067a, and RS-4110.2008.2. Use of the Advanced Photon Source was supported by the U. S. Department of Energy, Office of Science, Office of Basic Energy Sciences, under Contract No. DE-AC02-06CH11357.

REFERENCES

[1] Afanas'ev, A. M. and Kohn, V. G., "Dynamical Theory of X-Ray Diffraction in Crystals with Defects", Acta Cryst. A. 27, 421-430 (1971).

[2] Uragami, T. S., "Pendellösung Fringes in Bragg Case in a Crystal of Finite Thickness", J. Phys. Soc. Japan. 28, 1508-1527 (1970).

[3] Kohn, V. G., "Diffraction Reflection of a Focused X-ray Wave by a Multilayer Crystal ", Crystallogr. Rep., 51, 564-569 (2006).

[4] Kohn, V. G. and Kazimirov A., "Simulations of Bragg diffraction of a focused x-ray beam by a single crystal with an epitaxial layer", Phys. Rev. B., 75, 224119, 1-9 (2007).

[5] Snigirev, A., Kohn, V., Snigireva, I., Lengeler, B., "A compound refractive lens for focusing high-energy X-rays", Nature, 384, 49-51 (1996).

[6] Michette, A. G., "Optical systems for soft X-rays", Plenum Press, New York, London (1986).

[7] Cai, Z., Lai, B., Xiao, Y. and Xu S., "An X-ray diffraction microscope at the Advanced Photon Source", J. Phys. IV, 104, 17-20 (2003).

[8] SOI samples were purchased from Ultrasil Corporation, http://www.ultrasil.com.